

https://dspace.org/

Efficient electrooxidation of ammonia using platinum supported on titania/ sulfur-doped onion like carbon nanoparticles in direct ammonia fuel cells

Sikeyi, Ludwe L.; Bila, Laercia R.; Ntuli, Themba D.; Selepe, Cyril T.; Maxakato, Nobanathi W. ...

2023-02
Elsevier
https://hdl.handle.net/10539/50233
Ludwe L. Sikeyi, Laercia R. Bila, Themba D. Ntuli, Cyril T. Selepe, Nobanathi W. Maxakato, Neil J. Coville, Manoko S. Maubane-Nkadimeng, Efficient electrooxidation of ammonia using platinum supported on titania/sulfur-doped onion like carbon nanoparticles in direct ammonia fuel cells, Diamond and Related Materials, Volume 132, 2023, 109612, ISSN 0925-9635, https://doi.org/10.1016/j.diamond.2022.109612

Downloaded from a DSpace repository. https://dspace.org/

Diamond & Related Materials 132 (2023) 109612

Contents lists available at ScienceDirect

Diamond & Related Materials

journal homepage: www.elsevier.com/locate/diamond

Efficient electrooxidation of ammonia using platinum supported on titania/sulfur-doped onion like carbon nanoparticles in direct ammonia fuel cells

Ludwe L. Sikeyi [a], Laercia R. Bila [a], Themba D. Ntuli [a], Cyril T. Selepe [b], Nobanathi W. Maxakato [b], Neil J. Coville [a,c], Manoko S. Maubane-Nkadimeng [a,c,d,*]

[a] Molecular Sciences Institute, School of Chemistry, University of the Witwatersrand, Braamfontein 2050, South Africa
[b] Department of Chemical Sciences, University of Johannesburg, Doornfontein 2021, South Africa
[c] DSI-NRF Centre of Excellence in Strong Materials, University of the Witwatersrand, Braamfontein 2050, South Africa
[d] Microscopy and Microanalysis Unit, University of Witwatersrand, Braamfontein 2050, South Africa

ARTICLE INFO

Keywords:
Ammonia oxidation reactions
Cyclic voltammetry
Nano-catalysts
Onion-like carbon nanoparticles
Sulfur doping

ABSTRACT

This study reports on the synthesis of platinum supported on titania oxide nanoparticles decorated on sulfur doped onion-like carbon nanoparticles (S-OLCNs) as electrocatalysts for ammonia oxidation reactions in alkaline media. S-OLCNs (S = 1.6 %) were synthesized in a one-step flame pyrolysis method using thiophene as the starting material and titania nanoparticles were prepared using a microwave-assisted hydrolysis technique (5–10 % titania decoration). Pt/S-OLCN, Pt/TiO_2 and Pt/TiO_2/S-OLCN electrocatalysts (10 % Pt loading) were synthesized by the ethylene glycol assisted reduction method. Transmission electron microscopy studies confirmed the presence of well dispersed spherically shaped Pt NPs on the surface of the S-OLCN, TiO_2 and TiO_2/S-OLCN support materials (d = 1.93 ± 0.38 nm, 1.98 ± 0.79 nm, 2.13 ± 0.52 nm, respectively). XRD patterns confirmed the anatase phase for the titania. The Pt/S-OLCN, Pt/TiO_2 and Pt/TiO_2/S-OLCN and Pt/C electrocatalysts were investigated in the ammonia oxidation reaction (AOR). The existence of the well-dispersed TiO_2 (and Pt) on the S-OLCNs gave rise to enhanced AOR catalytic performance when compared to Pt/S-OLCN, Pt/TiO_2 and commercial 10 wt% Pt/C catalysts. Furthermore, the Pt/TiO_2/S-OLCN electrocatalyst exhibited better long term stability and a faster charge transfer resistance than Pt/S-OLCN, Pt/TiO_2 and commercial 10 wt% Pt/C electrocatalysts. These results indicate that the incorporation of TiO_2 nanoparticles into Pt/S-OLCN is an effective strategy to improve the AOR activity of Pt by facilitating the electron transfer process during the catalytic reactions.

1. Introduction

The electrochemical oxidation of ammonia has attracted much attention in recent years because of the effective use of ammonia as a fuel for electric energy generation in direct ammonia fuel cells (DAFCs) [1]. Ammonia as a liquid fuel is an excellent and appropriate chemical energy carrier since it is easy to handle under low pressure, has a high hydrogen density and can be easily oxidized into hydrogen and nitrogen at elevated temperatures [2]. Also, ammonia is easy to transport, produce, and store. The development of the alkaline DAFC has been used to convert ammonia into hydrogen (and nitrogen) under mild conditions, with ammonium hydroxide and potassium hydroxide used as a fuel and electrolyte respectively [3].

DAFCs have many advantages over alternative fuel cells such as the direct methanol fuel cell (DMFC). This is seen in terms of cost/type of the anode and the cathode kinetics [4]. The DAFC generates only nitrogen and water whereas the DMFC generates carbon dioxide (and hydrogen). The DAFC has a clear economic advantage as well, in that it is much faster, more efficient and is more cost effective when compared to the DMFC. The DAFCs do, however have some disadvantages such as: the ammonia electrocatalytic oxidation reaction is sluggish/slow require a high loading of the metal in the electrocatalyst to achieve acceptable reaction rates.

Pt is an example of the commonly used catalyst in a DAFC, because it provides a high electrocatalytic performance, good current density, long-term stability and excellent work functions [5]. However, its use has some limitations limited fuel cells, as Pt is expensive and there are limited Pt resources in the world and its applications have been limited

* Corresponding author at: Microscopy and Microanalysis Unit, University of Witwatersrand, Braamfontein 2050, South Africa.
E-mail address: manoko.maubane@wits.ac.za (M.S. Maubane-Nkadimeng).

https://doi.org/10.1016/j.diamond.2022.109612
Received 5 October 2022; Received in revised form 21 November 2022; Accepted 4 December 2022
Available online 9 December 2022
0925-9635/© 2022 Elsevier B.V. All rights reserved.

by two problems. These are: (i) the catalyst has a high overpotential (>0.5 V) and, (ii) it shows accelerated deactivation. Therefore, it is crucial to design new high performance nanocatalysts for the electrocatalytic oxidation of ammonia in fuel cells and at the same time to reduce the Pt loading in the electrocatalyst [6]. One way to achieve this is through the use of new catalyst support materials. Both carbon-based materials and metal oxides possess the required properties for their use as catalyst support materials [7]. These properties include: (i) high surface areas that are required for the dispersion of catalyst particles, (ii) the ability to conduct electricity, and (iii) the ability to maintain stability in reactions under ammonia electrocatalytic oxidation conditions.

Carbon materials such as conductive carbon, carbon nanotubes (CNTs), carbon black (CB), carbon nanofibers (CNFs), graphene (GR), carbon nano-onions (CNOs) etc., are the commonly used support materials for fuel cell electrocatalyst [8]. Recently, CNOs has attracted attention as a support material for metal nanoparticles in energy storage and conversions. Carbon nano-onions (CNOs) and heteroatom doped CNOs as well as their related onion-like carbon counterparts (OLCNs) are examples of support materials that that have used as catalyst supports in fuel cells [9]. CNOs and OLCNs are part of the multi-fullerene family; the OLCNs (sometimes referred to as CNOs) are made up of quasi-sphere-shaped and polyhedral shaped nano-graphitic layers of carbon atoms [10].

Doping with non-metal heteroatoms like sulfur, phosphorus, nitrogen and boron has been shown to increase the performance of carbon-based catalysts. This is due to the enhancement of the active sites in the graphitic framework together with interdependent coupling effects between heteroatoms [11]. Most studies on carbon doping have focused on the use of N, O and B dopants. Sulfur, like N and O act as an electron donor, and doping with sulfur has been shown to affect the electron density of states differently when compared to nitrogen doping [12].

Studies on the use of S-doped carbons in electrochemical reactions are well documented in literature. For example, Yang et al. reported the synthesis of S-doped graphene using benzyl disulfide as sulfur precursor and graphene oxide (GO) as carbon source. The electrochemical analysis of the S-doped graphene in alkaline electrolyte demonstrated an enhanced catalytic performance for oxygen reduction reaction (ORR) when compared to the standard Pt/C nanocatalyst [13]. In another study, Fan et al. reported on Pt nanoparticles loaded on sulfur doped carbon nanotubes that were prepared using an assisted autoclave method. The synthesized Pt/S-MWCNT electrocatalyst showed higher catalytic performance, CO-tolerance and improved long-term durability for the methanol oxidation reaction when compared to undoped Pt/MWCNT or a Pt/C commercial nanocatalyst (MOR) [14].

The performance of Pt-based electrocatalysts for ammonia oxidation reactions can be enhanced by modification of the carbon support materials by using carbons mixed with inorganic supports [15]. Inorganic metal oxides such MoO_3, SnO_2, CeO_2, WO_3, Al_2O_3, and TiO_2 have all been used as catalyst supports due to their higher stability in fuel cells [16–18]. In particular, TiO_2 (anatase phase) is regularly used as a support material because of its good specific surface area and strong interconnection with metal nanoparticles [19]. The addition of metal oxides, like TiO_2, to a standard Pt/C to generate Pt/TiOx/C nanocomposites have been shown to modify the electronic and structural properties of platinum [20]. A carbon-TiO_2 support has shown a high resistance to the electrochemical corrosion of carbon [20]. The TiO_2 modified the synergy between the carbon in the C-TiO_2 and the catalyst nanoparticles [21].

Interestingly, a recent study by Liu et al. revealed a preparation of Pt/TiO_2 nanotubes by the galvanostatic electrodeposition method [22]. On the other hand, while studying the ammonia oxidation reaction (AOR) on indium tin oxide (ITO) decorated with Pt nanoparticles, Li et al. revealed a high mass specific electrocatalytic activity of the Pt/ITO electrode towards AOR which was better than the commercial Pt/C electrode. This was ascribed to the effect of Pt nanoparticles (NPs) on the indium tin oxide substrate [23].

In this study, we present the use of S-doped onion-like carbon nanoparticles (S-OLCNs) as a carbon support and TiO_2/S-OLCN as a composite support material for Pt NPs in alkaline direct ammonia fuel cells. The S-OLCNs were synthesized from thiophene using the flame pyrolysis method, using methodology as reported in literature [24]. Platinum NPs were added to the surface of the S-OLCNs and TiO_2/S-OLCN support materials using the ethylene glycol reduction method. The sulfur functional groups are expected to facilitate the attachment of titania and platinum nanoparticles to the surface of the S-OLCNs. The synthesis of a TiO_2/S-OLCN structure could improve the anti-corrosion and anti-poisoning properties of the electrocatalyst. To the best of our knowledge, a detailed study on the TiO_2/S-OLCN support for platinum nanoparticles as electrocatalysts for direct ammonia fuel cells has not been previously reported. As discussed, the composite-modified (Pt/TiO_2/S-OLCN) electrode exhibited high catalytic performance for the oxidation of ammonia in alkaline electrolyte when compared to the Pt/S-OLCN, Pt/TiO_2 and a standard Pt modified electrode. The reasons for this finding are described.

2. Experimental

2.1. Materials

All chemicals were used as received to prepare the nanomaterials for the study: thiophene (99 %; Sigma-Aldrich), titanium butoxide (99.7 %; Sigma-Aldrich), ethanol (99.9 %; Sigma-Aldrich), acetylacetone (99.9 %; Sigma-Aldrich), sodium hydroxide (Sigma-Aldrich), ammonium sulphate (99 %; Sigma-Aldrich), dihydrogen hexachloroplatinate (98.0 %; Sigma-Aldrich), nafion solution (>5 wt%; Sigma-Aldrich), ethylene glycol (>99.9 %; Sigma-Aldrich), ammonium hydroxide (>30 %; Sigma-Aldrich), potassium hydroxide (>30 %; Sigma-Aldrich), 10 % Pt/C commercial standard (Sigma-Aldrich).

2.2. Synthesis of sulfur doped onion-like carbon nanoparticles (S-OLCNs)

S-OLCNs were synthesized using a simplified flame pyrolysis method as described by Mohapatra et al. [24]. From a typical laboratory-made design, 60 mL of thiophene (organic precursor) was placed into a 100 mL beaker and after ignition in air (in a fume hood) gave the S-OLCNs. Here, the thiophene acted as the sulfur source as well as the carbon source to produce the desired S-OLCNs. It was shown from a previous report that a flame could produce an appropriate high-temperature environment (800–1000 °C) that was effective for the preparation of pristine OLCNs. In this study, ignited thiophene (C_4H_4S) readily decomposed in air. Using a brass plate collector, the S-OLCNs were formed in the upper part of the flame. The product in the form of black carbon nanoparticles (S-OLCNs) were collected and a yield of 3.15 % was obtained. The S-OLCNs nanomaterial was used without additional post-processing or purification.

2.3. Synthesis of titanium dioxide (TiO_2) anatase

Titanium butoxide (2.0139 g) was dissolved into 20 mL of 99.9 % ethanol and 70 mL of deionized water. The solution was stirred for 30 min at 50 °C and a white suspension was obtained. Acetylacetone (10 mL) was added slowly into the resulting white suspension and the flask contents stirred for 30 min to complete the hydrolysis reaction. The white suspension was then transferred into a 100 ml Teflon reaction vessel and the vessel placed into an Anton Paar microwave reactor (750 W). The titanium suspension was then heated for 30 min at 180 °C. The resulting product from the microwave irradiation reaction was filtered and washed numerous times with double distilled water. The white solid that was obtained was dried in an oven at 100 °C overnight. The TiO_2 sample was calcined in a muffle furnace at 500 °C for 24 h to obtain TiO_2 anatase.

2.4. Synthesis of TiO_2/S-OLCN composite support material

S-OLCNs (400 mg) and TiO_2 anatase powder (26.7 mg) were dispersed in 60 mL of NaOH aqueous solution (10 M) and 10 mL of ammonium sulfate (1 M $(NH_4)_2SO_4$) solution using ultrasonication at 40 °C for 70 min (to produce a 10 % wt. TiO_2 loading on the S-OLCNs). The suspension was transferred into a Teflon-lined stainless-steel autoclave and kept at 200 °C for 24 h in a muffle furnace. The precipitate was cooled down naturally and collected using the 1000 mL Millipore filter system through a 0.22 μm polytetrafluoroethylene (PTFE) filter. The precipitate was washed thoroughly with deionized water a considerable number of times to remove any excess NH_4^+ ions, and then it was dried at 100 °C overnight. A light brown powder was obtained. The product was placed into a quartz boat that was calcined at 450 °C under argon for 2.5 h to obtain the TiO_2/S-OLCN composite support material.

2.5. Synthesis of Pt/S-OLCN, Pt/TiO_2, and Pt/TiO_2/S-OLCN electrocatalysts

The platinum-based nanocatalysts were prepared by the ethylene assisted reduction method [25]. In this procedure, 200 mg of each support (S-OLCN, TiO_2, and TiO_2/S-OLCN) was dispersed in 20 mL of ethylene glycol and 42.0 mg of H_2PtCl_6 (to produce a 10 % wt. Pt loading) was then added and the mixture stirred for 30 min. The obtained mixtures were sonicated in an ultrasound bath for another 30 min. The Pt/S-OLCN, Pt/TiO_2, and Pt/TiO_2/S-OLCN nanocatalysts solutions were then placed into three round bottom flasks and the solutions were then refluxed at 200 °C for 6 h. The resulting mixtures were centrifuged at 18000 rpm for 25 min and washed a considerable number of times with distilled water to eliminate residual chloride ions. The nanomaterials were dried at 100 °C for 24 h to obtain the Pt-based nanocatalysts.

2.6. Material characterization

The structure and morphology of the samples were recorded using a JEOL transmission electron microscope (TEM) model JEM-2100F operated at 200 kV. Surface micrographs and Energy dispersive X-rays (EDX) were obtained using a ZEISS Sigma 300 VP Oxford Field Emission Scanning Electron Microscope (SEM) instrument. The Fourier transform infrared (FTIR) spectra were obtained on a PerkinElmer Spectrum 100 instrument. Raman spectra of the OLCNs were acquired using a Raman spectrometer model Horiba Jobin Yvon with a laser wavelength of λ = 514 nm. The thermal stability of the samples was investigated using a Perkin Elmer 6000 thermogravimetric (TGA) analyzer. The specific surface areas and porosity characterization of the samples were analyzed using the Brunauer-Emmett-Teller method (BET) on a Micromeritics Tristar 3000 surface area analyzer. Powder X-ray diffraction (PXRD) patterns for the samples were obtained on a Bruker D2 Phaser diffractometer using a Cu Kα radiation source (λ = 0.15405 nm) generated at 30 kV and 10 mA. To determine the chemical states of the samples, X-ray photoelectron spectroscopy (XPS, Thermo Scientific ESCALAB 250Xi instrument) was performed with a high-resolution pass energy of 20 eV, monochromatic Al Kα (1486.7 eV) source.

2.7. Electrochemical measurements

Electrochemical measurements were investigated out using a Dropsens potentiostat. A glassy carbon (GC) electrode with a geometrical surface area of 0.196 cm^2 was utilized as a working electrode for the cyclic voltammetry (CV), chronoamperometry (CA), and electrochemical impedance spectroscopy (EIS) measurements. A platinum (Pt) wire was used as the counter electrode and a saturated silver/silver chloride electrode (Ag/AgCl) with a bridge tube as a reference electrode. The Ag/AgCl reference electrode cannot be used in ammonia buffer as Ag/AgCl forms a soluble complex with NH_3. The Ag/AgCl reference electrode was putted inside the bridge tube that had a ceramic glass frit to prevent the filling electrolyte (3.4 M KCl) doesn't leak into the sample; this also prevents contamination of the Pt counter electrode with ions such as chloride or potassium. Additionally, Pt is also susceptible to sulfur compounds, nitrogen compounds, and CO, leading to Pt poisoning due to strong chemisorption. Therefore, electrolyte purification to remove the poisonous impurities is necessary if Pt is chosen as the counter electrode. The working electrodes were prepared using an ink made of the electrocatalyst. This was done by dispersing 10 mg of nanocatalysts in 1 mL of isopropyl alcohol with 5 μL Nafion solution (5 wt%) and mixing for 15 min in an ultrasonic bath. After that, 15 μL aliquot of the electrocatalyst inks was pipetted onto the surface of the glassy carbon electrode and dried at ambient temperature. The loading of Pt in the electrocatalysts on the glassy carbon electrode is ca. 0.045 mg cm^{-2}. Prior to any electrochemical studies, the electrolyte solution was purged with argon for 20 min to remove any oxygen interference. CV, CA and EIS measurements were performed in solutions containing 1 M KOH and 1 M NH_4OH saturated with argon gas. For all Pt based electrocatalysts, the electroactive surface area (ECSA) values were normalized by the geometric surface area of the working (GC) electrode. Currents obtained in the CV and CA curves were normalized by the ECSA of the platinum based electrocatalysts.

3. Results and discussion

3.1. Physical characterization

3.1.1. Transmission electron microscopy (TEM)

A typical TEM micrograph of the TiO_2-anatase nanoparticles is given in Fig. S1(a) which shows the classical shape and agglomerated structure of anatase titania nanoparticles with an average diameter of 93.8 ± 11.5 nm (see Fig. S2(a)). The TEM micrograph depicted in Fig. 1(a) shows the as-synthesized S-OLCNs with an almost spherical morphology and the inset of SAED that confirms the presence of amorphous and fullerene like structure established on the basis of high magnification TEM. The onion-like concentric shell structure of the S-OLCNs was preserved even though the OLCNs were doped, which verified that the doping step did not alter the onion-like structure. The S-OLCNs contained disordered concentric graphitic multi-shells with an average diameter of 51.4 ± 8.27 nm as indicated in Fig. S2(b) [26]. A TEM image of the TiO_2/S-OLCN mixture is shown in Fig. 1(c) (and sup Fig. S1(c)). The data clearly shows that the material is comprised of a mixture of the two supports. It is not possible to determine the degree of interaction of the two components. TEM images of the carbon supports that contain Pt are also shown in Fig. 1(b) and (d) (Pt/S-OLCN and Pt/TiO_2/S-OLCN). Fig. 1(e) demonstrates the high resolution TEM image of Pt/TiO_2/S-OLCN nanomaterial. In Pt/TiO_2/S-OLCN, Pt nanoparticles showed the better crystallinity and *d*-spacing value of 0.23 nm (111), whereas TiO_2 anatase exhibits the fringe distance of 0.352 nm (Fig. S1(e)). Fig. 1 (f–g) represents the energy dispersive X-ray spectroscopy (TEM-EDX) spectra of Pt/TiO_2/S-OLCN captured on the selected area of sample. It clearly shows that Pt and TiO_2 nanoparticles are uniformly dispersed on S-OLCN surface. A TEM image of Pt supported on TiO_2 is shown in Sup Fig. S1(d). As seen in all images the Pt nanoparticles are well dispersed. A comparison of the data indicates that in the composite the Pt preferentially binds to the carbon (S-OLCNs), even though the composite contains 10 % TiO_2. The platinum nanoparticles appear to be marginally larger (2.13 ± 0.52 nm) when incorporated into the TiO_2/S-OLCN composite support, as compared to the S-OLCN support (1.93 ± 0.38 nm). A TEM micrograph of the Pt/TiO_2 nanomaterial is presented in Fig. S1(d) and also shows small platinum particles (1.98 ± 0.79 nm) well distributed on the titanium dioxide surface.

3.1.2. Scanning electron microscopy (SEM)

The SEM micrographs of the S-OLCNs, TiO_2/S-OLCN, Pt/OLCNs and Pt/TiO_2/S-OLCN nanomaterials are shown in Fig. 2. These images

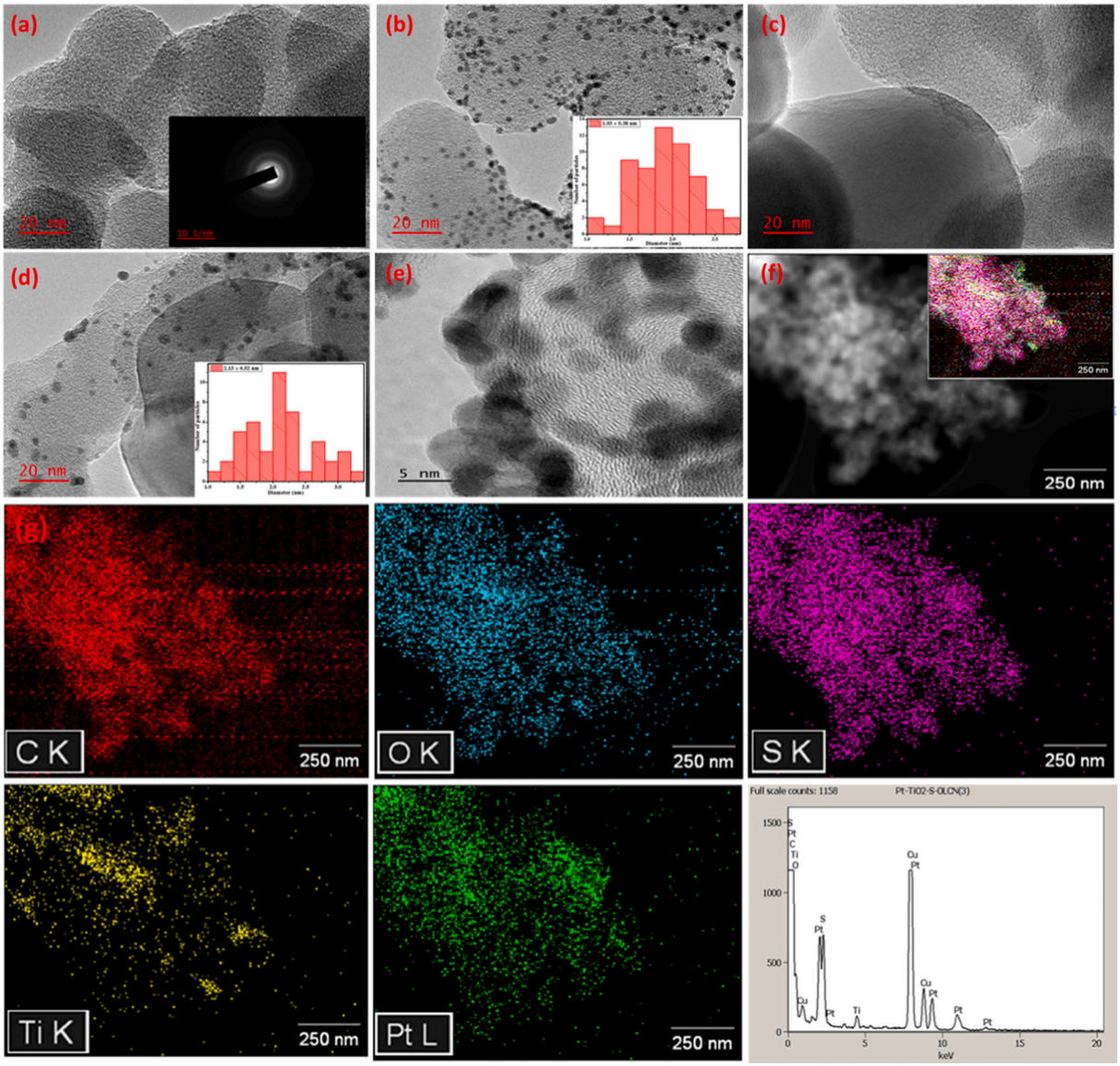


Fig. 1. High Magnification TEM micrographs of (a) S-OLCN, (b) Pt/S-OLCN and inset image of histogram representing Pt nanoparticle size is (1.93 ± 0.38 nm), (c) TiO_2/S-OLCN, (d) Pt/TiO_2/S-OLCN and inset image of histogram representing Pt nanoparticle size is (2.13 ± 0.52 nm), (e) high resolution TEM micrographs of Pt/TiO_2/S-OLCN, (f) HR-TEM image of selected area of Pt/TiO_2/S-OLCN and inset is corresponding EDX mapping represents the combination of elements in Pt/TiO_2/S-OLCN, (g) TEM-EDX elemental color mapping of the C, O, S, Ti, Pt elements.

display agglomerates of quasi-spherical morphology for the S-OLCNs [27] and the TiO_2 nanoparticles (Fig. 2 (a) and (b) respectively). The SEM image in Fig. 2 (b) also shows that the addition of the TiO_2 nanoparticles did not alter the morphology of the S-OLCNs.

Fig. 2 (c) and (d) shows the SEM images of Pt/S-OLCN and Pt/TiO_2/S-OLCN nanomaterials and indicated no significant changes in the sizes/shapes of the support particles. The TiO_2 anatase and Pt/TiO_2 images in Fig. S3 (a) and (b) consists of non-uniform shaped particles, which are conglomerates of large grains of the TiO_2. It can be observed that TiO_2 images show large particle sizes in the range between 60 nm and 140 nm diameter. The mixture of the two supports, with different sizes, is shown by the circles in the Fig. 2d. The image is dominated by the carbon, in agreement with the use of 10 % TiO_2. The Pt NPs were, as expected, not seen in the SEM images at the image resolution used.

3.1.3. Energy dispersive X-ray spectroscopy (EDS)

Elemental analyses of the S-OLCN, TiO_2/S-OLCN, Pt/S-OLCN and Pt/TiO_2/S-OLCN nanocomposite materials were studied using EDS. The EDS spectra shown in Fig. S4 (a and b), confirmed the presence of carbon, oxygen, sulfur, and titanium in the S-OLCN and TiO_2/S-OLCN support materials. Also, the EDS also confirmed the presence platinum in the Pt/S-OLCN (Fig. S4 (c)) and in Pt/TiO_2/S-OLCN (Fig. S4 (d)).

3.1.4. Fourier transform infrared and Raman spectroscopy

The FTIR spectrum of the S-OLCN is shown in Fig. 3. (a). The peak at 3416 cm^{-1} is due to a OH stretch mode. [28]. The peak at 1624 cm^{-1} is assigned to a C═C stretch in aryl rings [27]. The peak at 1404 cm^{-1} is attributed to the C—O—H stretch due to the existence of carboxylic functional groups [26] and the signal at 1109 cm^{-1} is assigned to a S═O/C—O stretching modes. This peak at 1109 cm^{-1} also consists of contributions from the S═O stretch (sulfoxide) and a C—O stretch (alcohol group) [29]. The large peaks of interest at 744 cm^{-1} and 611 cm^{-1} are assigned to a C—S and S—O stretching modes [30]. The FTIR data thus suggest that the S-OLCNs contain a carbon backbone structure and that the S-doping process did not damage the carbon framework.

Raman spectroscopy was used to ascertain the extent of structural

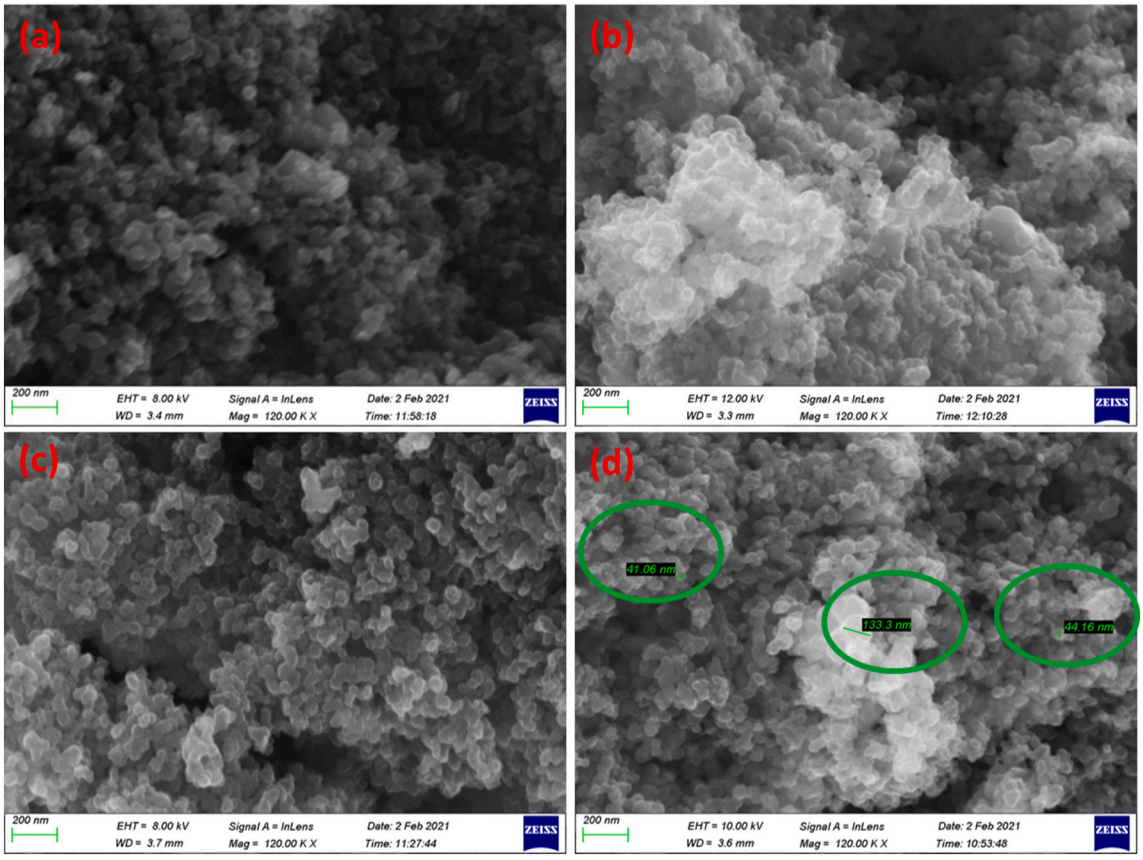


Fig. 2. Typical SEM micrographs of (a) S-OLCN (b) TiO_2/S-OLCN, (c) Pt/S-OLCN (d) Pt/TiO_2/S-OLCN nanomaterials.

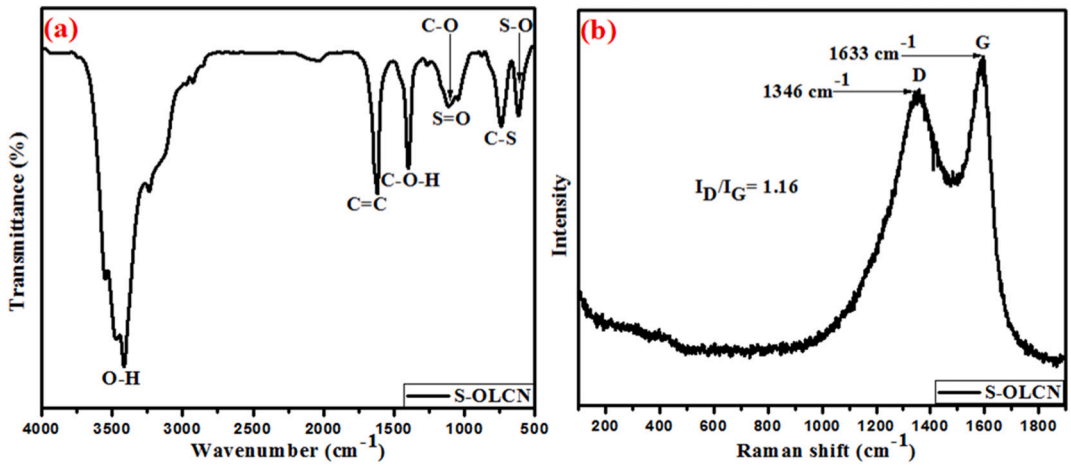


Fig. 3. (a) FTIR spectrum and (b) Raman spectrum of the S-OLCN nanomaterials.

imperfections in the graphitic carbon nanomaterial [24]. Fig. 3. (b), indicates the Raman spectra of the S-OLCN support material which showed two primary peaks. These were the D-band was found at 1346 cm^{-1} and the G-band at 1633 cm^{-1}. The D-band is associated with defects that are caused by doping, whilst the G-band is the result of the in-plane vibrational stretch of ordered sp^2-bonded carbon atoms. [31]. Thomas et al. reported that for their S-OLCN material, that the D-band (1335 cm^{-1}) and the G-band (1570 cm^{-1}) shifted downwards when compared to planar graphite. For example, the G-band got graphite typically occurs at 1582 cm^{-1} [32]. Interestingly, an upshift of the G-band was reported for p-CNO (ca. 1588 cm^{-1}) [26]. The reason for this upshift is suggested to be related to the tensile stress caused within the graphene planes by bending after doping [24]. The upshift confirmed the modifications of the carbon. The areas of the D and G bands were used to determine the I_D/I_G ratio, found to be 1.16. This I_D/I_G ratio was larger when compared to that reported by Mohapatra et al. (0.72) for a similar S-CNO material [24].

3.1.5. *Thermogravimetric analysis (TGA)*

The TGA and TGA derivative data were used to compare the stability of S-OLCN and TiO_2/S-OLCN, Pt/S-OLCN and Pt/TiO_2/S-OLCN nanomaterials under air in the temperature range of 35 °C–900 °C. As shown in Fig. S5 (b), the TGA derivative curve showed maximum decomposition temperatures of 643 °C and 577 °C for S-OLCNs and TiO_2/S-OLCN

respectively, which is ascribed to carbon thermal oxidation of the carbon [33]. The introduction of TiO_2 facilitated the thermal oxidation of the carbon. The residual weight of the TiO_2/S-OLCN was found to be 9.9 % and is due to the presence of TiO_2 nanoparticles.

The TGA and TGA derivative profiles of Pt/S-OLCN and Pt/TiO_2/S-OLCN indicated in Fig. 4. (367 °C and 382 °C for Pt/S-OLCN and Pt/TiO_2/S-OLCN (Fig. 4 (b)) are due to carbon oxidation. The introduction of Pt NPs increased the combustion of the carbon and hence lowered the thermal stability of the nanomaterials when compared to the non-Pt supports [34].

The residual weight of the Pt/TiO_2/S-OLCN was found to be 9.5 % and includes contributions from both TiO_2 and Pt. The residual weight of Pt/S-OLCN, due to the PtO_2 was found to be 5.8 %, suggesting that the TiO_2 content was ca 5 %. The residual weight obtained in both materials was less than the 10 % Pt theoretical loading.

3.1.6. X-ray diffraction spectroscopy (XRD)

Fig. 5 shows the X-ray diffraction patterns for the S-OLCN, TiO_2 anatase, Pt/S-OLCN, and Pt/TiO_2/S-OLCN nanomaterials. The XRD peak at $2\theta = 24.98°$ in the S-OLCN, Pt/S-OLCN, and Pt/TiO_2/S-OLCN spectra is attributed to the carbon (002) hexagonal structure while the intense diffraction peaks at $2\Theta = 39°$, 47°, 68° and 82° correlate to platinum (111), (200), (220), and (311) planes (JCPDS card. No 01-087-0646) [25]. The XRD pattern of TiO_2 indicates sharp peaks at $2\Theta = 25.6°$, 38.4°, 48.7°, 54.5°, 55.8°, 63.3°, 69.2°, 70.9°, 75.6°, 83.2° attributed to the TiO_2 anatase structure (JCPDS card. No 01-075-2544). The introduction of TiO_2 NPs to the carbon has negligible influence on the Pt crystal size of Pt/TiO_2/S-OLCN nanomaterial. The average crystallite size of the Pt/S-OLCN, and Pt/TiO_2/S-OLCN were estimated to be 2.2 nm, and 2.4 nm from the Pt (111) peak, using the Debye–Scherrer equation. Also, the average crystallite size of the TiO_2 anatase in Pt/S-OLCN-TiO_2 was found to be 94.5 nm from the TiO_2 (101) peak. These are similar to the data obtained from the TEM measurements. The mean crystallite size of the Pt nanoparticles of the platinum-based nanomaterials are also similar to those were reported by Ahmed et al. [35] and Wang et al. [40] that were used for methanol oxidation and oxygen reduction reactions, respectively.

3.1.7. X-ray photoelectron spectroscopy (XPS)

Fig. 6 (a) shows the XPS survey spectra of the Pt/TiO_2/S-OLCN and confirmed the existence of C 1s at 284.4 eV, O 1s at 532.6 eV, S 2p at 163.9 eV, Ti 2p at 458.7 eV and Pt 4f at 72.8 eV elements in the ternary composite nanomaterial. The elemental composition of the Pt/TiO_2/S-OLCN sample is shown in Table 1.

In Fig. 6 (b) the high-resolution XPS C1s spectrum of Pt/TiO_2/S-OLCN nanomaterial revealed six peaks. The two peaks that appeared at binding energies 284.1 and 284.9 eV correspond to sp^2 and sp^3 hybridized carbon atoms, respectively [36]. The peak at a binding energy of 285.6 eV is assigned to a C—S bond suggesting the binding of S to an sp^3 carbon atom [24]. The three peaks that appeared at binding energies 286.3, 287.5 eV and 288.8 eV are attributed to the C—O, C═O and O—C═O functional groups indicating the existence of carbonyl groups, respectively. The XPS spectrum of the oxygen O1s orbital shown in Fig. 6 (c), was deconvoluted into three peaks at 530.2 eV, 531.7 eV, and 532.9 eV which are ascribed to the Ti—O bond in anatase, and the C—O, and C═O carbonyl groups, respectively [37]. The high-resolution S2p spectrum showed peaks at ca 163 and 165 eV due to the presence of the expected $S2p_{1/2}$ and $S2p_{3/2}$ doublet in the correct ratio of ca. 1 to 2 (see Fig. 6 (d)). The location of the $S2p_{3/2}$ is consistent with RSH, C═S and C—S bonds, confirming the sulfur doping of the OLCN structure [24]. As can be seen in Fig. 6 (e), the Ti 2p XPS spectrum, exhibited spin-orbit coupling (1.0 eV) for Ti $2p^3$ at 459.2 eV suggesting the presence of a titanium (IV) species [38]. The XPS Pt 4f spectrum showed two distinct peaks for $Pt4f_{5/2}$ and $4f_{7/2}$ located at 71.2 eV and 74.5 eV, respectively, which can be deconvoluted into two peaks. The peaks located at 71.2 eV and 74.5 eV were attributed to metallic platinum (Pt^0) and Pt^{II} in Fig. 7 (f) [39]. The existence of the strong peaks for platinum Pt^{II} in the Pt4f spectra indicates the presence of oxidized Pt and a possible Pt-O-Ti interaction [40].

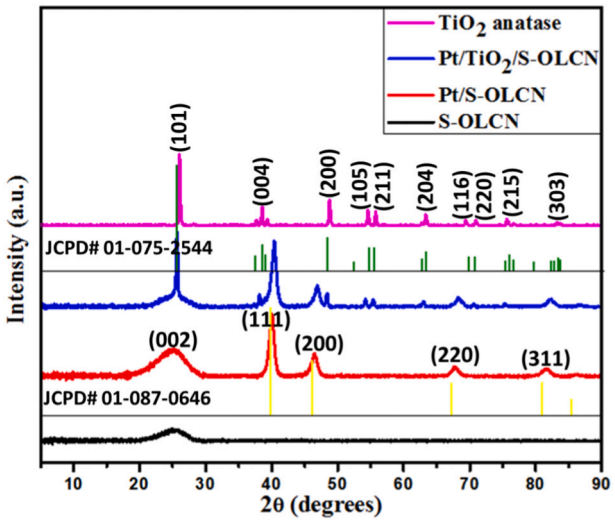


Fig. 5. X-ray diffractograms of S-OLCN, Pt/S-OLCN, Pt/TiO_2/S-OLCN, and TiO_2 anatase nanomaterials.

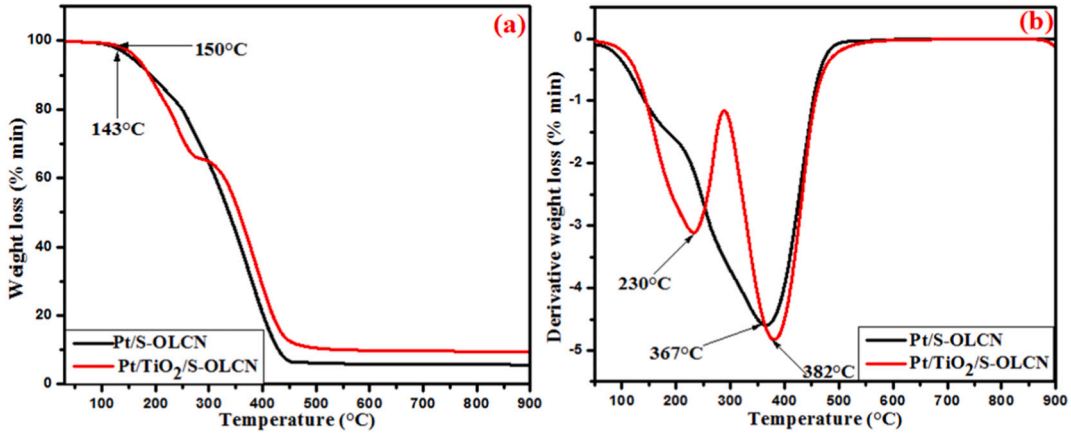


Fig. 4. (a) thermogravimetric analysis profiles and (b) differential thermogravimetric analysis curves of Pt/S-OLCN and Pt/TiO_2/S-OLCN nanomaterials.

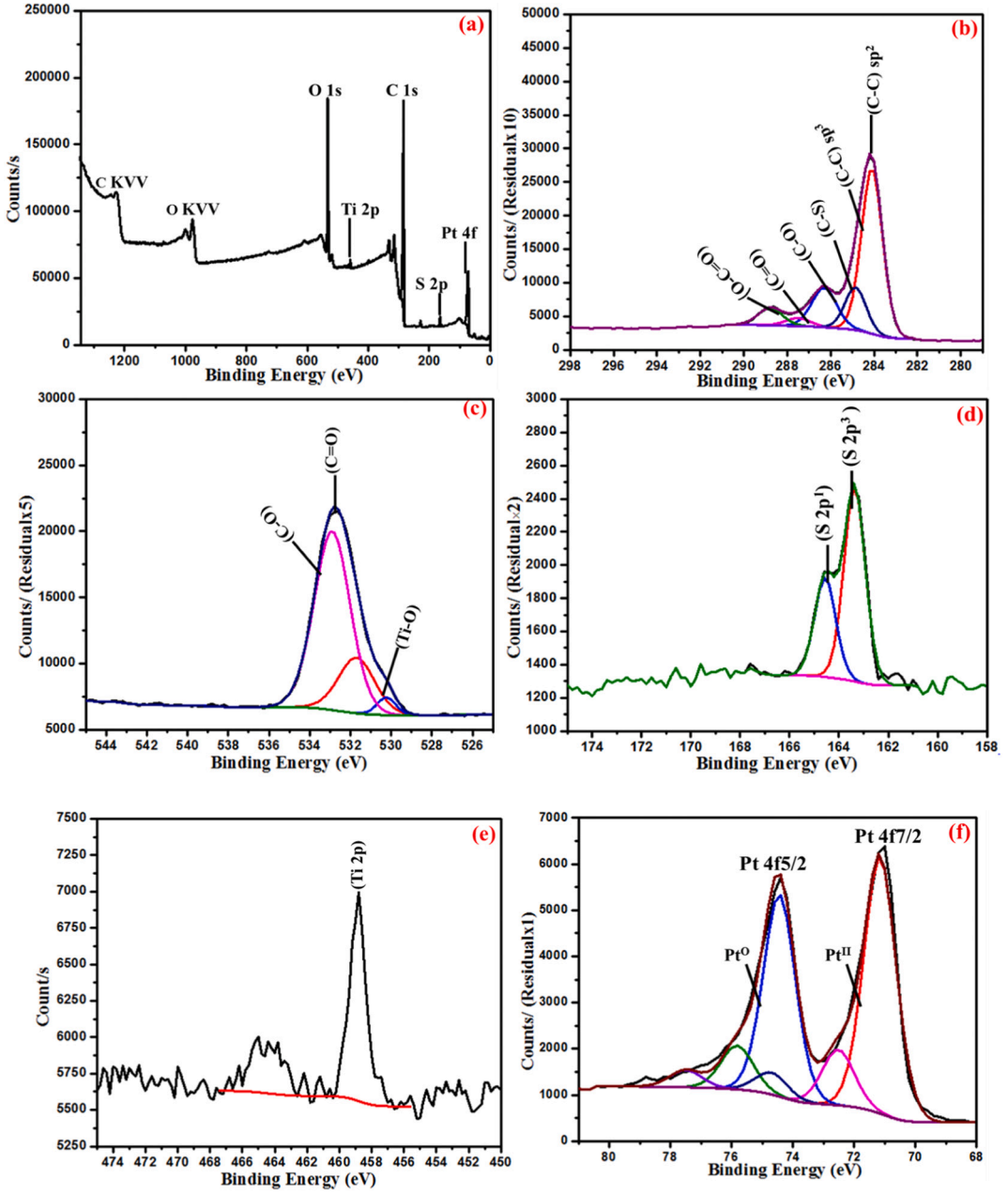


Fig. 6. XPS survey spectra of (a) Pt/TiO_2/S-OLCN (b) C 1s of Pt/TiO_2/S-OLCN (c) O 1s of Pt/TiO_2/S-OLCN (d) S 2p of Pt/TiO_2/S-OLCN (e) Ti 2p of Pt/TiO_2/S-OLCN and (f) Pt 4f of Pt/TiO_2/S-OLCN.

Table 1
Elemental composition of Pt/TiO_2/S-OLCN sample obtained from XPS data.

Sample	Carbon	Oxygen	Sulfur	Titanium	Platinum
Pt/TiO_2/S-OLCN	75.1	14.3	1.6	2.1	4.9

3.1.8. Brunauer-Emmett-Teller nitrogen adsorption (BET) data

The BET technique was used to measure the specific surface area of the nanomaterials Nitrogen adsorption-desorption isotherms and the pore size distribution data (derived from the desorption branch for Pt/S-OLCN and Pt/TiO_2/S-OLCN materials) are shown in Fig. S6. Table 2 lists the BET surface area data obtained for the electrocatalyst support materials. The BET surface area of S-OLCN was determined to be 55 $m^2\,g^{-1}$, which is higher than the TiO_2/S-OLCN (27 $m^2\,g^{-1}$), Pt/TiO_2 (34 $m^2\,g^{-1}$), Pt/S-OLCN (46 $m^2\,g^{-1}$) and Pt/TiO_2/S-OLCN (52 $m^2\,g^{-1}$) electrocatalysts. Presumably this is due to the Pt and TiO_2 nanoparticles which have been well dispersed and block the pores of the S-OLCN catalyst support surface [41].

3.2. Electrocatalytic behaviour of the Pt based electrocatalysts

3.2.1. Electrochemical surface area (ECSA)

The electrochemically active surface area (ECSA) of the Pt/C, Pt/TiO_2, Pt/S-OLCN and Pt/TiO_2/S-OLCN nanocatalysts was determined using cyclic voltammetry (CV) recorded at a scan rate of 50 mVs^{-1} in 1 M KOH solution (Fig. 7). The electrocatalyst currents were normalized using the geometric area of the working electrode. ECSA of the Pt-based nanocatalysts was estimated from Eq. (1) [33].

$$ECSA_{Pt,cat}\left[m^2g^{-1}\right] = \frac{Q_H[mC]}{Q_{density}[mCcm^{-2}] \times L_{metal}[mg]} \quad (1)$$

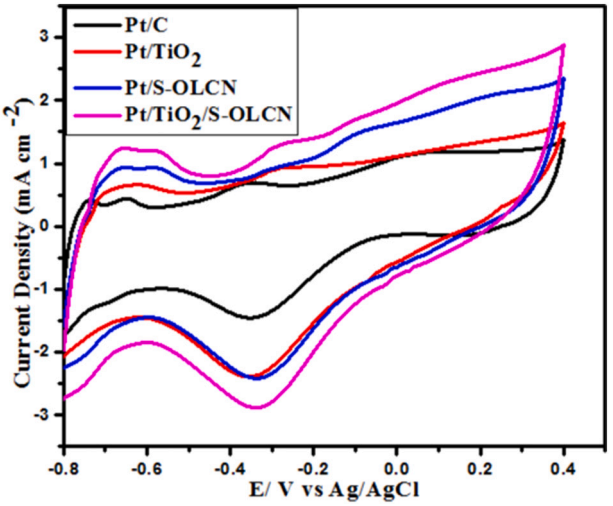


Fig. 7. (a) CV curves for the Pt/C, Pt/TiO_2, Pt/S-OLCN and Pt/TiO_2/S-OLCN nanocatalysts in 1 M KOH at a scan rate of 50 mV s^{-1}.

Table 2
BET surface area of the platinum supported on sulfur-doped onion like carbon nanoparticles-titania nanomaterials.

Sample	Surface area (m^2g^{-1})	Pore volume (cm^3g^{-1})
S-OLCN	55	0.19
S-OLCN-TiO_2	27	0.28
Pt/S-OLCN	46	0.31
Pt/TiO_2/S-OLCN	52	0.34
Pt/TiO_2	34	0.10

The CV curves of the four electrocatalysts are very similar to that of polycrystalline Pt, which displayed distinctive potential regions including the H-adsorption/desorption peaks, the double layer peak and the Pt oxide formation/reduction peaks. All the Pt-based nanocatalysts exhibited hydrogen adsorption/desorption peaks between −0.8 and −0.5 V (vs Ag/AgCl), which are ascribed to the adsorption/desorption of both weakly and strongly bonded hydrogen species.

The ECSA data followed the order: Pt/TiO_2/S-OLCN (49.89 m^2 g^{-1}) > Pt/S-OLCN (45.13 m^2 g^{-1}) > Pt/TiO_2 (41.37 m^2 g^{-1}) > Pt/C (36.52 m^2 g^{-1}). The enhanced ECSA of the Pt/TiO_2/S-OLCN can be ascribed to the generation of new active sites at the interface between Pt and TiO_2 NPs, enhanced by the S-OLCNs [42,43].

3.2.2. Cyclic voltammetry (CV)

CVs were measured in ammonia-containing solution at a scan rate 50 mV s^{-1} and the data are shown in Fig. 8 for the Pt/C, Pt/TiO_2, Pt/S-CNO and Pt/TiO_2/S-OLCN modified electrodes. The reported currents were normalized using the ECSA data. The cyclic voltammograms (in 1 M KOH + 1 M NH_4OH solution) displayed voltammetric profiles that are very similar to the one obtained for the Pt-NCs prepared by the polyol method [44]. The ammonia oxidation peaks are clearly seen for the four electrocatalysts at around −0.51 to −0.16 E/V vs Ag/AgCl. It is observed that the onset potential for ammonia oxidation reaction on commercial Pt/C catalyst (−0.492 V vs Ag| AgCl) has higher values than the ones obtained using Pt/TiO_2/S-OLCN, Pt/S-OLCN and Pt/TiO_2 catalysts. Surprisingly, the Pt/S-OLCN and Pt/TiO_2 (−0.514 V vs Ag|AgCl) nanocatalysts has the same lower values of onset potential as compared to Pt/TiO_2/S-OLCN (−0.501 V vs Ag|AgCl) nanocatalysts for ammonia oxidation in alkaline electrolyte. These lower onset potentials confirm that the Pt nanoparticles had been successfully dispersed on the surface of the TiO_2/S-OLCN. It is suggested that the different interactions with these support materials modified the electronic structure of Pt, causing the easier catalysis and dissociation of ammonia [37].

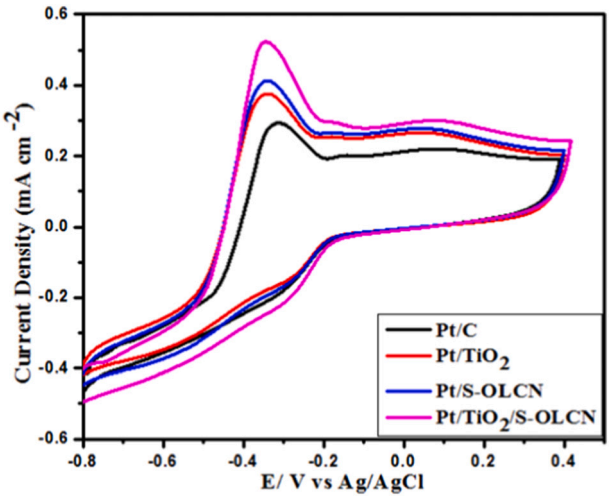


Fig. 8. CV curves of the Pt/C, Pt/TiO_2, Pt/S-OLCN and Pt/TiO_2/S-OLCN modified electrodes in 1 M KOH + 1 M NH_4OH at a scan rate of 50 mV s^{-1}.

The CV curves showed the following order: Pt/TiO_2/S-OLCN (0.52 mA cm^{-2}) Pt/S-OLCN > (0.41 mA cm^{-2}) > Pt/TiO_2 (0.38 mA cm^{-2}) > Pt/C (0.33 mA cm^{-2}). These results demonstrate the enhanced catalytic performance of the sulfur doped carbon in Pt/TiO_2/S-OLCN electrocatalyst. The larger ECSA of Pt/TiO_2/S-OLCN could supply more active sites for the AOR and improve the electrocatalytic efficiency. In addition, the Pt/TiO_2/S-OLCN electrocatalysts shows higher catalytic activity as compared to our previous study of the synthesized undoped Pt/p-OLCN (0.13 mA cm^{-2}) electrocatalyst [33]. This is attributed to the surface wettability and hydrophilicity of S-OLCNs support, which improve interactions between the electrolyte ions, the analyte and the surface of the electrode [45]. The dissociative adsorption of water molecules on the titanium dioxide support material generated Ti—OH surface groups. These Ti—OH groups near the Pt nanoparticles may promote the removal of nitrogenous groups bonded on the Pt atoms (Pt-N_{ads} poisoning interaction) which was modified by the TiO_2 support [22]. According to Liu et al. Pt/titanium dioxide nanotube showed enhanced electrocatalytic performance towards AOR process in the ammonia activation and adsorption under UV-light illumination, [22]. A comparative analysis of catalytic performance of the nanocatalysts reported in this study with other similar Pt/C catalysts for the electrochemical ammonia oxidation reactions is revealed in Table 3. It is evident that the synthesized nanocatalysts in general shows better catalytic activity towards AOR than the other nanocatalysts listed.

3.2.3. Chronoamperometry (CA)

The CA measurements of the Pt/C, Pt/TiO_2, Pt/S-OLCN and Pt/TiO_2/S-OLCN modified electrodes, were also carried out in the solution of 1 M KOH containing 1 M NH_4OH at a constant potential of −0.3 V. As shown in Fig. 9, the current density for the ammonia oxidation reactions on all

Table 3
Comparison of Pt/TiO_2, Pt/S-OLCN and Pt/TiO_2/S-OLCN to other Pt/C catalysts reported for ammonia oxidation reactions.

Electrocatalysts	Fuel (M)	Electrolyte (M)	CD (mA cm^{-2})	Ref.
Pt/TiO_2/S-OLCN	1 NH_4OH	1 KOH	0.52	This work
Pt/S-OLCN	1 NH_4OH	1 KOH	0.41	This work
Pt/TiO_2	1 NH_4OH	1 KOH	0.38	This work
Pt/TiO_2 nanotubes	0.1 NH_3	1 KOH	0.36	[22]
Pt/MnO_2	0.2 NH_4OH	1KOH	0.51	[46]
Pt/SnO_2/C	0.5 NH_4OH	1 KOH	0.71	[1]

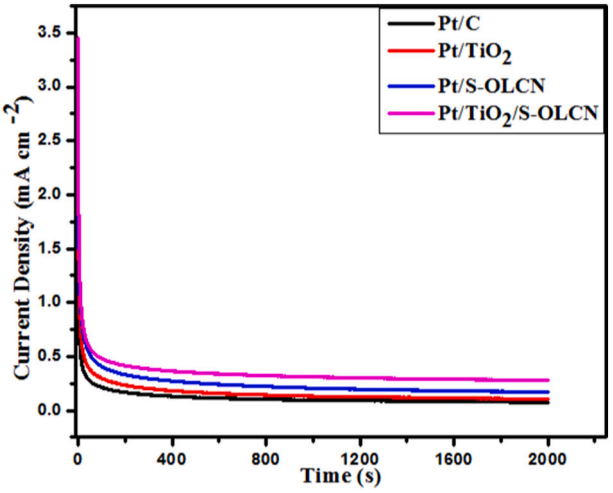


Fig. 9. CA curves for Pt/C, Pt/TiO_2, Pt/S-OLCN and Pt/TiO_2/S-OLCN electrocatalysts in 1 M KOH + 1 M NH_4OH at the potential peak of the ammonia oxidation.

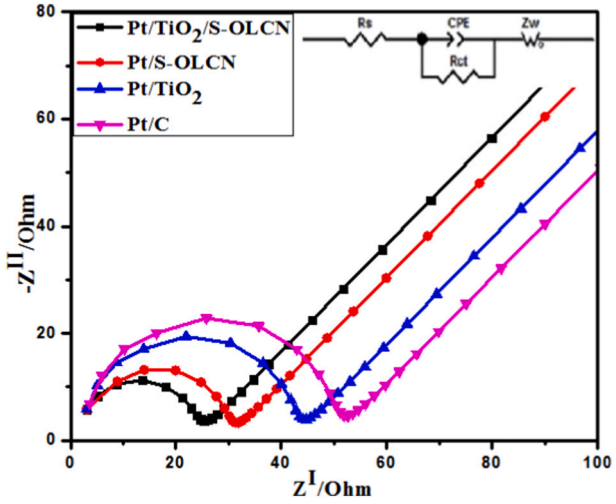


Fig. 10. Nyquist plots of Pt/C, Pt/TiO_2, Pt/S-OLCN and Pt/TiO_2/S-OLCN electrocatalysts in 1 M KOH + 1 M NH_4OH and along with the equivalent circuit (inset).

four electrocatalysts gradually decreased and then became stable with the increasing time. The current density after 2000 s of measurement followed the order: Pt/TiO_2/S-OLCN (0.28 mA cm^{-2}) > Pt/S-OLCN (0.17 mA cm^{-2}) > Pt/TiO_2 (0.11 mA cm^{-2}) > Pt/C (0.09 mA cm^{-2}). The improved catalytic activity of Pt/TiO_2/S-OLCN electrocatalyst is ascribed to the strong metal−support interaction between platinum nanoparticles and S-OLCN-TiO_2 composite support material [47]. Also, this could be due to the "spill over" effect whereby adsorbed intermediates on the Pt sites move to neighbouring Ti-OH species to assist in accelerated oxidation [48]. Titanium dioxide assists the platinum catalyst in avoiding deactivation form nitrogen intermediates (Pt-N_{ads}) that poisoning the Pt formed during the ammonia oxidation reaction process [22]. Additionally, the strong electron transfer interconnection from the Pt NPs to the S groups in onion structure will change the electronic state of the Pt catalyst surface [49] and thus improve the catalytic activity of Pt/TiO_2/S-OLCN towards the AOR.

3.2.4. *Electrochemical impedance spectroscopy (EIS)*

EIS measurements were carried out to investigate the electrode/electrolyte interface resistance and the reaction kinetics of the Pt-based nanocatalysts towards the ammonia oxidation in alkaline electrolyte. Nyquist plots at the constant potential of −0.2 V of the Pt/C, Pt/TiO_2, Pt/S-OLCN and Pt/TiO_2/S-OLCN modified electrodes in Ar saturated of 1 M KOH containing 1 M NH_4OH solution are shown in Fig. 10. Nyquist impedance plots of the Pt-based electrocatalysts from 1000 kHz to 0.005 Hz were recorded. The relevant parameters (solution resistance (Rs), charge transfer resistance (RCT) and Warburg impedance (Zw)) are summarized in Table 4, [50]. The Nyquist impedance arc is shown in Fig. 10, the data show that the Pt/TiO_2/S-OLCN electrocatalyst exhibits the faster charge transmission and highest conductivity. These results are consistent with the catalytic activity obtained from the CV and CA data.

Table 4
Electrochemical impedimetric data of Pt/C, Pt/TiO_2, Pt/S-OLCN and Pt/TiO_2/S-OLCN electrocatalysts.

1 M KOH + 1 M NH_4OH				
Electrocatalysts	R_s (Ohm)	R_{ct} (Ohm)	CPE (μF)	Z_W (Ω s − 1/2)
Pt/C	21.5 ± 0.45	51.2 ± 3.32	164.9 ± 8.61	6.0E-06
Pt/TiO_2	19.9 ± 0.41	43.1 ± 2.95	158 ± 9.24	8.0E-06
Pt/S-OLCN	13.8 ± 0.47	30.9 ± 3.75	172 ± 5.34	5.0E-06
Pt/TiO_2/S-OLCN	11.1 ± 0.42	24.7 ± 3.63	167.6 ± 7.48	7.0E-06

4. Conclusions

In this study, sulfur doped onion-like carbon nanoparticles (S-OLCNs) were successfully synthesized in a one-step flame pyrolysis method using thiophene as both the carbon and sulfur source. The TiO_2/S-OLCN composite support material was designed to have well dispersed titania nanoparticles on a carbon nano onion surface using a hydrothermal reaction process. The ultrafine Pt nanoparticles were successfully deposited on the S-OLCN, TiO_2 and TiO_2/S-OLCN surfaces by the alcohol assisted reduction method. The TEM, XRD and XPS results confirmed the formation of highly decorated ultrafine Pt NPs with an average diameter of 2.0 nm that were strongly bonded to the S-OLCN, TiO_2 and TiO_2/S-OLCN framework. The ternary composite-modified (Pt/TiO_2/S-OLCN) electrode demonstrated higher catalytic performance, better long-term stability and smaller charge transfer resistance for the ammonia oxidation reaction in alkaline medium as compared to Pt/S-OLCN, Pt/TiO_2, and Pt/C modified electrodes. It was suggested that the superior electrocatalytic performance resulted from a strong Pt-support interaction and the better accessibility of ultrafine Pt nanoparticles to the reactants on the TiO_2/S-OLCN composite support material. A protecting effect of TiO_2/S-OLCN towards Pt that evades the adsorption of ammonia and nitrogenous intermediates on the platinum surface was observed. Therefore, the Pt/TiO_2/S-OLCN electrocatalyst is a good anode electrocatalyst for ammonia tolerant-oxidation reaction in direct alkaline fuel cells. Further studies to explore this electrocatalyst type are underway.

CRediT authorship contribution statement

Ludwe L Sikeyi: Investigation, Writing-Original Draft, Validation.
Laercia Bila: Methodology.
Themba D Ntuli: Data Curation.
Cyril T Selepe: software.
Nobanathi W Maxakato: Resources, Supervision.
Neil J Coville: Writing- Reviewing and Editing, Resources, Supervision.
Manoko S Maubane-Nkadimeng: Conceptualization, Resources, Supervision.

Declaration of competing interest

The authors declare that they have no known competing financial interests or personal relationships that could have appeared to influence the work reported in this paper.

Data availability

Data will be made available on request.

Acknowledgments

This work is based on the research supported in part by the National Research Foundation (NRF) of South Africa (Grant Numbers: 138075, 118137, 118148), the University of the Witwatersrand (Postgraduate Merit Award, University Research Council) and a NRF-DAAD grant (Grant number: 117841). The authors also acknowledge the efforts and support provided by the University of Johannesburg (Faculty of Science, University Research Council, and Centre for Nanomaterials Science Research). We also wish to acknowledge Mr. Siyasanga Mpelane at the University of Johannesburg (Auckland Park) for the high magnification TEM data.

Appendix A. Supplementary data

Supplementary data to this article can be found online at https://doi.org/10.1016/j.diamond.2022.109612.

References

[1] J.R. Barbosa, M.N. Leon, C.M. Fernandes, R.M. Antoniassi, O.C. Alves, E.A. Ponzio, J.C.M. Silva, PtSnO2/C and Pt/C with preferential (100) orientation: high active electrocatalysts for ammonia electro-oxidation reaction, Appl. Catal. B Environ. 264 (2020), https://doi.org/10.1016/j.apcatb.2019.118458.
[2] L.A. Diaz, G.G. Botte, Mathematical modeling of ammonia electrooxidation kinetics in a polycrystalline pt rotating disk electrode, Electrochim. Acta 179 (2015) 519–528, https://doi.org/10.1016/j.electacta.2014.12.162.
[3] K. Endo, Y. Katayama, T. Miura, Pt–Ir and Pt–Cu binary alloys as the electrocatalyst for ammonia oxidation, Electrochim. Acta 49 (2004) 1635–1638, https://doi.org/10.1016/j.electacta.2003.11.024.
[4] Y. Zhao, B.P. Setzler, J. Wang, J. Nash, T. Wang, B. Xu, Y. Yan, An efficient direct ammonia fuel cell for affordable carbon-neutral transportation, Joule 3 (2019) 2472–2484, https://doi.org/10.1016/j.joule.2019.07.005.
[5] J.C.M. Silva, S.G. Da Silva, R.F.B. De Souza, G.S. Buzzo, E.V. Spinacé, A.O. Neto, M. H.M.T. Assumpção, PtAu/C electrocatalysts as anodes for direct ammonia fuel cell, Appl. Catal. A Gen. 490 (2015) 133–138, https://doi.org/10.1016/j.apcata.2014.11.015.
[6] C. Zhong, W.B. Hu, Y.F. Cheng, Recent advances in electrocatalysts for electro-oxidation of ammonia, J. Mater. Chem. A 1 (2013) 3216–3238, https://doi.org/10.1039/c2ta00607c.
[7] M.J. Lázaro, S. Ascaso, S. Pérez-Rodríguez, J.C. Calderón, M.E. Gálvez, M.J. Nieto, R. Moliner, A. Boyano, D. Sebastián, C. Alegre, L. Calvillo, V. Celorrio, Carbon-based catalysts: synthesis and applications, C. R. Chim. 18 (2015) 1229–1241, https://doi.org/10.1016/j.crci.2015.06.006.
[8] X. Chen, F. He, Y. Shen, Y. Yang, H. Mei, S. Liu, T. Mori, Y. Zhang, Effect of carbon supports on enhancing mass kinetic current density of fe-N/C electrocatalysts, Chem. Eur. J. 23 (2017) 14597–14603, https://doi.org/10.1002/chem.201703020.
[9] A. Shaikh, B.K. Singh, D. Mohapatra, S. Parida, in: Nitrogen-Doped Carbon Nano-Onions as a Metal-Free Electrocatalyst, 2019, pp. 222–231.
[10] V. Dhand, M. Yadav, S.H. Kim, K.Y. Rhee, A comprehensive review on the prospects of multi-functional carbon nano onions as an effective, high-performance energy storage material, Carbon N. Y. 175 (2021) 534–575, https://doi.org/10.1016/j.carbon.2020.12.083.
[11] A. Camisasca, A. Sacco, R. Brescia, S. Giordani, Boron/Nitrogen-codoped carbon Nano-onion electrocatalysts for the oxygen reduction reaction, ACS Appl. Nano Mater. 1 (2018) 5763–5773, https://doi.org/10.1021/acsanm.8b01430.
[12] A. Priyadarsini, B.S. Mallik, Effects of doped N, B, P, and S atoms on graphene toward oxygen evolution reactions, ACS Omega 6 (2021) 5368–5378, https://doi.org/10.1021/acsomega.0c05538.
[13] S. Graphene, M.C. Catalyst, O. Reduction, Sulfur-doped graphene as an e ffi cient metal-free cathode catalyst for, ACS Nano 6 (2012) 205–211.
[14] J.J. Fan, Y.J. Fan, R.X. Wang, S. Xiang, H.G. Tang, S.G. Sun, A novel strategy for the synthesis of sulfur-doped carbon nanotubes as a highly efficient pt catalyst support toward the methanol oxidation reaction, J. Mater. Chem. A 5 (2017) 19467–19475, https://doi.org/10.1039/c7ta05102f.
[15] T.L. Lomocso, E.A. Baranova, Electrochemical oxidation of ammonia on carbon-supported bi-metallic PtM (M = ir, pd, SnOx) nanoparticles, Electrochim. Acta 56 (2011) 8551–8558, https://doi.org/10.1016/j.electacta.2011.07.041.
[16] P. Munnik, P.E. De Jongh, K.P. De Jong, Recent developments in the synthesis of supported catalysts, Chem. Rev. 115 (2015) 6687–6718, https://doi.org/10.1021/cr500486u.
[17] F. Chekin, S. Bagheri, S.B. Abd Hamid, Synthesis of pt doped TiO2 nanoparticles: characterization and application for electrocatalytic oxidation of l-methionine, Sensors Actuators B Chem. 177 (2013) 898–903, https://doi.org/10.1016/j.snb.2012.12.002.
[18] C. Martín, G. Solana, P. Malet, V. Rives, Nb2O5-supported WO3: a comparative study with WO3/Al2O3, Catal. Today 78 (2003) 365–376, https://doi.org/10.1016/S0920-5861(02)00301-2.
[19] S. Bagheri, N.Muhd Julkapli, S.Bee Abd Hamid, Titanium dioxide as a catalyst support in heterogeneous catalysis, Sci. World J. 2014 (2014), https://doi.org/10.1155/2014/727496.
[20] B. Ruiz-Camacho, O. Martínez-Álvarez, H.H. Rodríguez-Santoyo, V. Granados-Alejo, Pt/C and Pt/TiO2-C electrocatalysts prepared by chemical vapor deposition with high tolerance to alcohols in oxygen reduction reaction, J. Electroanal. Chem. 725 (2014) 19–24, https://doi.org/10.1016/j.jelechem.2014.04.019.
[21] S.S. Gwebu, T. Matthews, W.N. Maxakato, Pt nanoparticles on carbon nanodots-titania composite for enhanced electro oxidation of alcohol fuels, J. Electrochem. Energy Convers. Storage 19 (2022) 1–8, https://doi.org/10.1115/1.4050000.
[22] J. Liu, B. Liu, Z. Ni, Y. Deng, C. Zhong, W. Hu, Improved catalytic performance of Pt/TiO2 nanotubes electrode for ammonia oxidation under UV-light illumination, Electrochim. Acta 150 (2014) 146–150, https://doi.org/10.1016/j.electacta.2014.10.119.
[23] S. Li, H. Chen, J. Liu, Y. Deng, X. Han, W. Hu, C. Zhong, Size- and density-controllable fabrication of the platinum Nanoparticle/ITO electrode by pulse potential electrodeposition for ammonia oxidation, ACS Appl. Mater. Interfaces 9 (2017) 27765–27772, https://doi.org/10.1021/acsami.7b08604.
[24] D. Mohapatra, G. Dhakal, M.S. Sayed, B. Subramanya, J.J. Shim, S. Parida, Sulfur doping: unique strategy to improve the supercapacitive performance of carbon Nano-onions, ACS Appl. Mater. Interfaces 11 (2019) 8040–8050, https://doi.org/10.1021/acsami.8b21534.
[25] S. Meenakshi, K.G. Nishanth, P. Sridhar, S. Pitchumani, Spillover effect induced pt-TiO2/C as ethanol tolerant oxygen reduction reaction catalyst for direct ethanol fuel cells, Electrochim. Acta 135 (2014) 52–59, https://doi.org/10.1016/j.electacta.2014.04.142.
[26] L.L. Sikeyi, T.D. Ntuli, T.H. Mongwe, N.W. Maxakato, E. Carleschi, B.P. Doyle, N. J. Coville, M.S. Maubane-Nkadimeng, Microwave assisted synthesis of nitrogen doped and oxygen functionalized carbon nano onions supported palladium nanoparticles as hybrid anodic electrocatalysts for direct alkaline ethanol fuel cells, Int. J. Hydrog. Energy 46 (2021) 10862–10875, https://doi.org/10.1016/j.ijhydene.2020.12.154.
[27] T.D. Ntuli, T.H. Mongwe, L.L. Sikeyi, O. Mkhari, N.J. Coville, E.N. Nxumalo, M. S. Maubane-Nkadimeng, Removal of hexavalent chromium via an adsorption coupled reduction mechanism using olive oil derived carbon nano-onions, Environ. Nanotechnol. Monit. Manag. 16 (2021), 100477, https://doi.org/10.1016/j.enmm.2021.100477.
[28] O. Butsyk, P. Olejnik, E. Romero, M.E. Plonska-Brzezinska, Postsynthetic treatment of carbon nano-onions: surface modification by heteroatoms to enhance their capacitive and electrocatalytic properties, Carbon N. Y. 147 (2019) 90–104, https://doi.org/10.1016/j.carbon.2019.02.063.
[29] H. Sun, G. Li, A. Xu, Z. Xu, S. Wu, Sulfur-doped hollow soft-balled mesoporous carbon particles as ultra-fast, durable hosts for potassium storage, J. Alloys Compd. 906 (2022), 164311, https://doi.org/10.1016/j.jallcom.2022.164311.
[30] S.R. Kamali, C.N. Chen, D.C. Agrawal, T.H. Wei, Sulfur-doped carbon dots synthesis under microwave irradiation as turn-off fluorescent sensor for Cr(III), J. Anal. Sci. Technol. 12 (2021), https://doi.org/10.1186/s40543-021-00298-y.
[31] Y. Qiu, J. Huo, F. Jia, B.H. Shanks, W. Li, N- and S-doped mesoporous carbon as metal-free cathode catalysts for direct biorenewable alcohol fuel cells, J. Mater. Chem. A 4 (2015) 83–95, https://doi.org/10.1039/c5ta06039g.
[32] K. Bogdanov, A. Fedorov, V. Osipov, T. Enoki, K. Takai, T. Hayashi, V. Ermakov, S. Moshkalev, A. Baranov, Annealing-induced structural changes of carbon onions: high-resolution transmission electron microscopy and raman studies, Carbon N. Y. 73 (2014) 78–86, https://doi.org/10.1016/j.carbon.2014.02.041.
[33] L.L. Sikeyi, T.D. Ntuli, T.H. Mongwe, N.W. Maxakato, N.J. Coville, M.S. Maubane-Nkadimeng, Platinum nanoparticles loaded on pristine and boron oxide modified carbon Nano-onions for enhanced ammonia electrooxidation in alkaline direct ammonia fuel cells, J. Electroanal. Chem. 917 (2022), 116411, https://doi.org/10.2139/ssrn.3982297.
[34] V. Mashindi, P. Mente, N. Mpofu, T.N. Phaahlamohlaka, O. Makgae, A.I. Kirkland, R. Forbes, K.I. Ozoemena, P.B. Levecque, N.J. Coville, Platinum supported on pristine and nitrogen-doped bowl-like broken hollow carbon spheres as oxygen reduction reaction catalysts, J. Appl. Electrochem. (2021), https://doi.org/10.1007/s10800-021-01554-0.
[35] L.M. Ahmed, I. Ivanova, F.H. Hussein, D.W. Bahnemann, Role of platinum deposited on TiO2 in photocatalytic methanol oxidation and dehydrogenation reactions, Int. J. Photoenergy 2014 (2014), https://doi.org/10.1155/2014/503516.
[36] Q. Zhang, W. Huang, J. Ming Hong, B.Y. Chen, Deciphering acetaminophen electrical catalytic degradation using single-form S doped graphene/Pt/TiO2, Chem. Eng. J. 343 (2018) 662–675, https://doi.org/10.1016/j.cej.2018.02.089.
[37] J. Wang, M. Xu, J. Zhao, H. Fang, Q. Huang, W. Xiao, T. Li, D. Wang, Anchoring ultrafine pt electrocatalysts on TiO2-C via photochemical strategy to enhance the

stability and efficiency for oxygen reduction reaction, Appl. Catal. B Environ. 237 (2018) 228–236, https://doi.org/10.1016/j.apcatb.2018.05.085.
[38] K. Zhang, J. Qiu, J. Wu, Y. Deng, Y. Wu, L. Yan, Morphological tuning engineering of Pt@TiO2/graphene catalysts with optimal active surfaces of support for boosting catalytic performance for methanol oxidation, J. Mater. Chem. A 10 (2022) 4254–4265, https://doi.org/10.1039/d1ta09359b.
[39] R. Cui, S. Liu, X. Guo, H. Huang, J. Wang, B. Liu, Y. Li, D. Zhao, J. Dong, B. Sun, N-doping holey graphene TiO2-pt composite as efficient electrocatalyst for methanol oxidation, ACS Appl. Energy Mater. 3 (2020) 2665–2673, https://doi.org/10.1021/acsaem.9b02364.
[40] Y. Guo, L. Tang, Y. Zhang, H. Wei, X. Shu, J. Cui, Y. Wang, J. Liu, Q. Li, X. Sun, Y. Wu, Construction of three-dimensional hierarchical Pt/TiO2@C nanowires with enhanced methanol oxidation properties, Int. J. Hydrog. Energy 45 (2020) 33440–33447, https://doi.org/10.1016/j.ijhydene.2020.09.052.
[41] Y. Pei, Y. Niu, W. Zhang, Y. Zhang, J. Ma, Z. Li, Ionic liquid microemulsion mediated synthesis of Pt/TiO2 nanocomposites for ammonia borane hydrolysis, Int. J. Hydrog. Energy 47 (2022) 2819–2831, https://doi.org/10.1016/j.ijhydene.2021.10.215.
[42] L. Xiong, A. Manthiram, Synthesis and characterization of methanol tolerant Pt/TiOx/C nanocomposites for oxygen reduction in direct methanol fuel cells, Electrochim. Acta 49 (2004) 4163–4170, https://doi.org/10.1016/j.electacta.2004.04.011.
[43] H.J. Kim, D.Y. Kim, H. Han, Y.G. Shul, PtRu/C-Au/TiO2 electrocatalyst for a direct methanol fuel cell, J. Power Sources 159 (2006) 484–490, https://doi.org/10.1016/j.jpowsour.2005.10.101.
[44] H.Y. Sun, G.R. Xu, F.M. Li, Q.L. Hong, P.J. Jin, P. Chen, Y. Chen, Hydrogen generation from ammonia electrolysis on bifunctional platinum nanocubes electrocatalysts, J. Energy Chem. 47 (2020) 234–240, https://doi.org/10.1016/j.jechem.2020.01.035.
[45] D. Mohapatra, G. Dhakal, M.S. Sayed, B. Subramanya, J. Shim, S. Parida, Sulfur doping : unique strategy to improve the supercapacitive performance of carbon nano-onions, ACS Appl. Mater. Interfaces 11 (2019) 8040–8050, https://doi.org/10.1021/acsami.8b21534.
[46] S. Ntais, A. Serov, N.I. Andersen, A.J. Roy, E. Cossar, A. Allagui, Z. Lu, X. Cui, E. A. Baranova, P. Atanassov, Promotion of ammonia electrooxidation on pt nanoparticles by nickel oxide support, Electrochim. Acta 222 (2016) 1455–1463, https://doi.org/10.1016/j.electacta.2016.11.124.
[47] O. Dulub, W. Hebenstreit, U. Diebold, Imaging cluster surfaces with atomic resolution: the strong metal-support interaction state of pt supported on TiO2 (110), Phys. Rev. Lett. 84 (2000) 3646–3649, https://doi.org/10.1103/PhysRevLett.84.3646.
[48] S.S. Gwebu, P.N. Nomngongo, N.W. Maxakato, Pt/CNDs-TiO2 electrocatalyst for direct alcohol fuel cells, Mater. Today Proc. 5 (2018) 10460–10469, https://doi.org/10.1016/j.matpr.2017.12.377.
[49] Q. Zhang, W. Huang, J. Ming Hong, B.Y. Chen, Deciphering acetaminophen electrical catalytic degradation using single-form S doped graphene/Pt/TiO2, Chem. Eng. J. 343 (2018) 662–675, https://doi.org/10.1016/j.cej.2018.02.089.
[50] E. Hernández-Balaguera, H. Vara, J.L. Polo, An electrochemical impedance study of anomalous diffusion in PEDOT-coated carbon microfiber electrodes for neural applications, J. Electroanal. Chem. 775 (2016) 251–257, https://doi.org/10.1016/j.jelechem.2016.06.007.